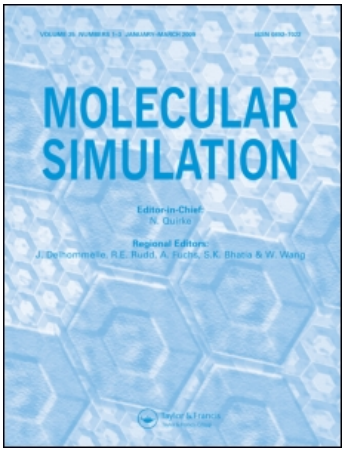


**Molecular Simulation**
Publication details, including instructions for authors and subscription information:
http://www.informaworld.com/smpp/title~content=t713644482

# Mechanical, rheological and transport properties of soft particle fluids

D. M. Heyes[a]; A. C. Brańka[b]
[a] Division of Chemistry, School of Biomedical and Molecular Sciences, University of Surrey, Guildford, UK [b] Institute of Molecular Physics, Polish Academy of Sciences, Poznan, Poland

**To cite this Article** Heyes, D. M. and Brańka, A. C.(2005) 'Mechanical, rheological and transport properties of soft particle fluids', Molecular Simulation, 31: 13, 945 — 959
**To link to this Article: DOI:** 10.1080/08927020500378006
**URL:** http://dx.doi.org/10.1080/08927020500378006

*Molecular Simulation*, Vol. 31, No. 13, 15 November 2005, 945–959

Taylor & Francis
Taylor & Francis Group

# Mechanical, rheological and transport properties of soft particle fluids

D. M. HEYES†* and A. C. BRAŃKA‡¶

†Division of Chemistry, School of Biomedical and Molecular Sciences, University of Surrey, Guildford GU2 7XH, UK
‡Institute of Molecular Physics, Polish Academy of Sciences, Smoluchowskiego 17, Poznan 60-179, Poland

*(Received September 2005; in final form September 2005)*



In this report, we investigate the physical and dynamical properties of model fluids whose constituent particles have their softness varied in a systematic manner. Molecular dynamics (MD) computer simulation is applied to inverse power or soft-sphere fluids, in which the particles interact through the pair potential, $\phi(r) = \epsilon(\sigma/r)^n$ where $n$ measures the steepness or stiffness of the potential. We have investigated the properties of model fluids with $4 \leq n \leq n = 1152$ over a wide density range. Attention is paid to local structural properties, the elastic moduli and the transport coefficients (principally the shear viscosity, $\eta_s$ and self-diffusion coefficient, $D$). We note that this is the first time mechanical and transport coefficient data have been reported for $n = 4$. It was found that the Batschinski–Hildebrand expressions, in which $D$ and $\eta_s^{-1}$ are assumed to have a linear dependence on the molar volume, represent the data quite well for all $n$. The density for which, on extrapolation, each of these quantities are zero, increases with the softness of the interaction (or $\sim n^{-1}$), suggesting that the effective hard sphere diameter decreases with increasing softness in the small $n$ limit. This treatment leads to simple empirical formulas for the effect of density (in an intermediate range) and $n$ on the two transport coefficients of these fluids. As $n$ decreases so do the relative fluctuations in the pressure and force on a particle. The local coordination number as measured up to the first minimum in the radial distribution function does not increase significantly above $\simeq 13$ up to the co-existence packing fluid, even for the softest of particles (i.e. $n = 4$). If we assume that the effective hard sphere diameter is approximately the position of the first peak in the radial distribution function, the Stokes–Einstein expression reproduces the simulation data reasonably well, with the boundary condition being typically between the stick and slip limits, and approaching the latter with increasing density. For the softer particles and with increasing packing fraction, the shear viscosity increases more rapidly than the self-diffusion coefficient decreases. For the softer systems, the bulk viscosity is relatively low compared to the shear viscosity, in contrast to the trend for the corresponding infinite frequency moduli. The softer particles are more "rubbery" in their response (relatively high bulk modulus compared to the shear modulus), which leads us to conclude that auxetic behaviour is more likely to arise when the building units are quite hard.

*Keywords*: Auxetic behaviour; Bulk modulus; Packing fraction; Stokes–Einstein expression

## 1. Introduction

There are a number of physical properties that we assume implicitly to be positive, but can be negative. An example is Poisson's ratio, which according to the classical theory of elasticity for isotropic three-dimensional materials can be in the range $-1 \leq \nu \leq 1/2$, restricted between these bounds by the fact that both the bulk and shear moduli be positive (a Poisson's ratio of $1/2$ indicates the useful case in theory of an incompressible system). An auxetic material is one with a negative Poisson's ratio [1,2]. Stretched in one direction, it expands rather than contracts (as one usually expects) along at least one perpendicular direction. Similarly, a contraction along one dimension causes a contraction along at least one perpendicular direction. Auxetic behaviour is usually associated with solids, but the effect has been observed for an example of a liquid crystal polymer [3], in which the architecture of the molecule confers the auxetic properties. Auxetic materials have many potential applications, such as skin bandaids as they allow the wound to "breathe" when the band is stretched [4]. They are also effective at absorbing the energy of impacts (e.g. for use in gymnastic mats and body armour). One could argue that, for example, cardboard boxes that are auxetic, are best referred to as "structures" or "frameworks". In contrast, if the auxetic effect

*Corresponding author. Email: d.heyes@surrey.ac.uk
¶Email: branka@ifmpan.poznan.pl

*Molecular Simulation*
ISSN 0892-7022 print/ISSN 1029-0435 online © 2005 Taylor & Francis
http://www.tandf.co.uk/journals
DOI: 10.1080/08927020500378006

originates at the molecular level, these are best referred to as "materials". The distinction is largely one of the characteristic lengthscale of the body compared to the human scale of perception.

Materials with negative Poisson's ratio are rare in nature, and despite considerable progress, the construction of materials with $\nu < 0$ is still quite a challenge, especially where we require the effect to originate at a molecular level. This is because materials exhibiting this behaviour have to undergo a certain type of (recoverable and reversible) concerted displacement of the structural members. Most of the modelling to date has concentrated on idealized microstructures which by cooperative motion of the members exhibit expansion when they are stretched, such as the re-entrant honeycomb structure [5–7]. Recently, auxetic behaviour has been obtained without re-entrant structures through the relative rotation of rigid (e.g. tetrahedral) units [8]. These two mechanisms for the auxetic effect share in common a synchronization or translational–rotational coupling of the constituent rigid units to produce the effect [8]. Although, the individual or component members of an auxetic material have themselves a high degree of rigidity, the assembly taken as a whole is "compliant" in the orthogonal stretch/compress action. Auxetic materials are characterised by a relatively high shear modulus but low bulk modulus; in contrast to rubbery materials which have a large bulk modulus but small shear modulus.

Although, auxetic materials do not fall into the class of simple liquids or solids, as the effect relies on the coupled motion of the constituent building units, it is possible that viewed on a coarse-grained level the microstructure could be represented by "blobs" with some specified radial and tangential effective interactions, as has been quite successfully achieved for granular materials [9]. As a first step, it is therefore of interest to have a better characterisation of the physical and dynamical properties of assemblies of particles with variable softness, which is the subject of this work. We consider the inverse power potential,

$$\phi(r) = \epsilon\left(\frac{\sigma}{r}\right)^n, \tag{1}$$

where $r$ is the separation between two particles, $\sigma$ is the particle diameter, $\epsilon$ sets the energy scale and $n$ is a parameter determining the potential steepness (the softness is $\varepsilon \sim n^{-1}$). The softness of the potential can be "tuned" by varying the exponent $n$. The softest particle we consider is with $n = 4$, which is the lowest integer value for which the integral formulae defining the various thermodynamic quantities and infinite frequency elastic moduli converge [10]. As $n \to \infty$, the potential in equation (1) tends to the hard sphere potential, $\phi_{\rm HS}(r) = \infty$, $r \leq d$, $= 0$, $r > d$, where $d$ is the hard sphere diameter and in the $n \to \infty$ limit, $\sigma = d$. The phase diagram of the soft-sphere system for variable $n$ has been computed by Agrawal and Kofke using Gibbs–Duhem integration [11]. MD simulation has been used to compute the dynamical behaviour (time correlation functions) and transport coefficients of these fluids for $n = 12$–$1152$ [12–16]. The time correlation functions associated with the shear and bulk viscosity, and thermal conductivity (as required in the Green-Kubo formulas) were calculated as a function of $n$ (see [17,18]). The main conclusion was that, when $n$ is large, the effects of the interaction "stiffness" (i.e. the value of $n$ here) on the short time part of the time correlation functions can be accounted for by a "renormalization" of the actual time by multiplication by the exponent $n$. These time correlation functions collapse at short times, up to $nt \sim 1$, using this scaled time definition. For lower values of $n$, say, 18–72 scaling can be better achieved with a more detailed scaling condition, $x = n(1 + (L/n))^{1/2}t$, where $L$ depends on state point [19]. The first term accounts for the leading two-body contributions to the relaxation, and the second term, in $L$, represents additional two-body and the leading three body contribution. $L$ depends mainly on the packing fraction and weakly on $n$ for *ca.* $n \geq 18$.

The transport coefficients are hardly distinguishable from those of hard spheres if $n$, exceeds *ca.* 72. For the static properties, the sensitivity to $n$ depends on the highest order ($q$th) derivative of the pair potential in the expression. For the $q$th order derivative, the property will vary for large $n$ as $\propto n^{q-1}$. The potential energy, pressure and infinite frequency elastic moduli correspond to $q = 0, 1$ and 2, respectively. The pressure ($q = 1$) case is, therefore, something of a fluke, as its sensitivity to $n$ is very weak for large $n$. This nevertheless is a welcome feature as it means that the equation of state is relatively insensitive to $n$ for large $n$. On either side of the pressure (in terms of $q$), the potential energy ($q = 0$) varies as $\sim n^{-1}$ and the infinite frequency elastic moduli ($q = 2$) go as $\sim n$.

From its definition in equation (1), it can be seen that the inverse power potential is a self-similar function, which mixes the energy and distance scales. It can be simply represented as $r^{*-n}$, where $r^* = (r/\sigma\epsilon)^{1/n}$. Because of the scaling properties of the potential, we can define a temperature scaled distance, $\tilde{r} = r\sigma^{-1}(\beta\epsilon)^{-(1/n)}$. The excess thermodynamic properties can be expressed in terms of a temperature-scaled density, $\tilde{\rho} = (\beta\epsilon)^{(3/n)}\rho\sigma^3$, where $\rho = N/V$ is the number density for $N$ particles in volume $V$. Similarly, for the packing fraction we have, $\tilde{\zeta} = (\beta\epsilon)^{(3/n)}\zeta$ which is used to characterize the density of the system. The scaled time is $\tilde{t} = t\sigma^{-1}\epsilon^{1/2}m^{-1/2}(\beta\epsilon)^{-(1/2)-(1/n)}$. In addition, we have the following reduced quantities, for the potential energy, $\tilde{u} = \beta u = \tilde{r}^{-n}$ and for pressure $\tilde{P} = P\epsilon^{-1}\sigma^3(\beta\epsilon)^{1+(3/n)}$. The scaled self-diffusion coefficient is $\tilde{D} = D\sigma^{-1}\epsilon^{-1/2}m^{+1/2}(\beta\epsilon)^{(1/2)-(1/n)}$. The scaled shear viscosity is $\tilde{\eta}_s = \eta_s\sigma^2\epsilon^{-1/2}m^{-1/2}(\beta\epsilon)^{(1/2)+(2/n)}$, with the same scaling for the bulk viscosity. The thermal conductivity is $\tilde{\lambda} = \lambda\sigma^2\epsilon^{-1/2}m^{-1/2}(\beta\epsilon)^{(1/2)+(2/n)}$. For conciseness, when presenting results and in the graphical annotation, we omit the ~ notation. These reduced quantities are obtained by carrying out the simulations at a reduced temperature $T^* = k_{\rm B}T/\epsilon = 1$,

where $k_B$ is Boltzmann's constant and $T$ is the temperature, or equivalently, $\beta\epsilon = 1$. The quantities, $\tilde{D}$, $\tilde{\eta}_s$, $\tilde{\eta}_b$ and $\tilde{\lambda}$ are numerically equal to $D^*$, $\eta_s^*$, $\eta_b^*$ and $\lambda^*$, respectively, obtained under these conditions.

## 2. Theory

### 2.1 Thermodynamic properties

The potential energy per particle, $u$, is an especially important quantity for the $r^{-n}$ fluids, as other static properties can be written in terms of it, when combined with several other system parameters. For an $N$ particle periodic system we can obtain $u$, from a molecular simulation using the following average,

$$u = \frac{1}{2N}\left\langle \sum_{i=1}^{N}\sum_{j=1,j\neq i}^{N} \phi_{ij}(r_{ij}) \right\rangle, \tag{2}$$

where $r_{ij}$ is the separation between particles $i$ and $j$ and $\langle\cdots\rangle$ denotes an ensemble (Monte–Carlo) or time (MD) average. $u$ can also be written in terms of the radial distribution function of the continuous potential system, $g(r)$,

$$u = 2\pi\rho\int_0^\infty g(r)\phi(r)r^2\,\mathrm{d}r. \tag{3}$$

Perturbation theory is a way to make analytical progress (e.g. see [20] for a general discussion of perturbation theory). In previous publications, we have used this approach, where the properties of the soft system are expanded about that of a notional "equivalent" hard sphere fluid with diameter, $\sigma_{HS}$, which (unlike for "true" hard spheres) is temperature dependent and can be density dependent. (As $n\to\infty$, $\sigma_{HS}\to\sigma$ for all temperatures.) This gives, [18]

$$\frac{u}{k_BT} = \frac{3(Z_{HS}-1)}{n} + O(n^{-2}), \tag{4}$$

where $Z_{HS}$ is the compressibility factor ($\equiv PV/Nk_BT$) for the hard sphere fluid at an equivalent hard sphere packing fraction, $\zeta = \pi N\sigma_{HS}^3/6V$. There are a number of accurate equations of state of the hard sphere fluid $Z_{HS}$ in the literature which are perfectly adequate for use in equation (4) (e.g. [21,22]) Note the strong sensitivity of $u/k_BT$ to $n$, and that in the hard sphere ($n\to\infty$) limit $u\to 0$, as it should. Similarly, for the pressure $P$, [18]

$$P = \rho k_BT - \frac{2\pi\rho^2}{3}\int_0^\infty \mathrm{d}r\, g(r) r^3 \frac{\mathrm{d}\phi}{\mathrm{d}r}. \tag{5}$$

we find $Z \simeq Z_{HS} + O(n^{-1})$, i.e. a relatively weak $n$-dependence. This treatment only works well near the hard sphere limit, and for very soft fluids it appears that a hard sphere reference fluid approach can still be used, after adding in a correction for the difference in available configurational space between the hard and soft systems [10]. The scaling behaviour of the soft sphere potential, also is manifest in the cavity function, $y(r) = g(r)\exp(\phi(r)/k_BT)$, which goes as $\sim r^{-C}$ in the region of "contact" of the spheres ($C$ depends on density and $n$) [23–25].

We now consider applications of this general treatment to static properties associated with transport coefficients and dynamical processes in liquids.

### 2.2 Time correlation functions and elastic properties

To calculate a transport coefficient, $\chi$, in MD a Green-Kubo formula can be used,

$$\chi = A\int_0^\infty \langle B(s+t)B(s)\rangle_s\,\mathrm{d}t, \tag{6}$$

where $\langle\cdots\rangle_s$ is a time correlation function at time $t$ averaged over a sampling time, $s$ which is the simulation time in practice. Here, $\chi$ is either the bulk or shear viscosity or the thermal conductivity. The property $B$ denotes the shear stress for the shear viscosity, $P(t) - \langle P\rangle$, where $P(t)$ is the instantaneous pressure and $\langle P\rangle$ is the average pressure, for the bulk viscosity and denotes the heat flux for the thermal conductivity. The constant $A$ is a combination of numerical factors, and basic quantities such as the volume of the system, the temperature and Boltzmann's constant. It is convenient to define a normalised time correlation function,

$$C(t) = \langle B(s+t)B(s)\rangle_s / \langle B^2(s)\rangle_s, \tag{7}$$

chosen so that $C(0) = 1$. Substitution of equation (7) in (6) gives,

$$\chi = C_\infty\int_0^\infty C(t)\,\mathrm{d}t, \tag{8}$$

where

$$C_\infty = A\langle B^2\rangle. \tag{9}$$

From the shear stress correlation function, the infinite frequency shear rigidity modulus is $C_\infty \equiv G_\infty = (V/k_BT)\langle P_{xy}^2\rangle$ [14], where $P_{xy}$ is an off-diagonal element of the pressure tensor. For the pressure correlation function, $C_\infty \equiv K_\infty - K_0 = (V/k_BT)\langle(P - \langle P\rangle)^2\rangle$ [14], the difference between the infinite and zero frequency bulk moduli [14]. Therefore, $\chi = C_\infty\tau$ where $\tau = \int_0^\infty C(t)\,\mathrm{d}t$ is a relaxation time, which is of the form proposed by Maxwell for the shear stress relaxation function and viscosity of gases [26] (he assumed an exponential relaxation function).

Work to date in the series of publications concerning the $r^{-n}$ fluids has concentrated on the various transport coefficients and the associated time correlation functions. The shear viscosity was considered first [12,13], and then more recently by Rickayzen *et al.* [27]. We have discussed the bulk viscosity [14] and the heat flux autocorrelation function $C_T(t)$ [15] which gives the thermal conductivity in a Green-Kubo formula.

The infinite frequency elastic moduli are static averages, given in terms of pair-wise interactions by the following formulae [28],

$$G_\infty = \rho k_B T + \frac{2\pi\rho^2}{15}\int_0^\infty \mathrm{d}r\, g(r)\frac{\mathrm{d}}{\mathrm{d}r}\left(r^4\frac{\mathrm{d}\phi}{\mathrm{d}r}\right), \quad (10)$$

and

$$K_\infty = \frac{2\rho k_B T}{3} + P + \frac{2\pi\rho^2}{9}\int_0^\infty \mathrm{d}r\, g(r) r^3 \frac{\mathrm{d}}{\mathrm{d}r}\left(r\frac{\mathrm{d}\phi}{\mathrm{d}r}\right), \quad (11)$$

For the inverse power potentials, the pressure and mechanical properties can be written in terms of $u$, defined in equation (3). The interaction part of the pressure is given by,

$$P^u \equiv P - \rho k_B T = n\rho u/3, \quad (12)$$

and the interaction part of the infinite frequency shear rigidity modulus is given by,

$$G_\infty^u \equiv G_\infty - \rho k_B T = \frac{(n^2-3n)\rho u}{15}$$

$$= \frac{1}{5}(n-3)(P-\rho k_B T). \quad (13)$$

Using the definition of the packing fraction, $\zeta = \pi\rho\sigma^3/6$ we have,

$$G_\infty \sigma^3 = \frac{6}{\pi}\zeta k_B T + \frac{12}{5\pi} n(n-3)\zeta u. \quad (14)$$

The interaction part of the infinite frequency bulk compressional modulus is given by,

$$K_\infty^u \equiv K_\infty - \frac{5}{3}\rho k_B T = \frac{(n^2+3n)\rho u}{9}$$

$$= \frac{1}{3}(n+3)(P-\rho k_B T), \quad (15)$$

by using equation (12) to eliminate $u$. Similarly, to equation (14),

$$K_\infty \sigma^3 = \frac{10}{\pi}\zeta k_B T + \frac{2}{3\pi} n(n+3)\zeta u. \quad (16)$$

Note that equations (14) and (16) are exact expressions for the two moduli. The moduli diverge as $\propto n$ for large $n$ values (as $u \propto n^{-1}$, see equation (4)), and are infinite in the $n \to \infty$ hard-sphere limit. For large $n$ and at any state point, $K_\infty/G_\infty \simeq 5/3$. For smaller $n$, the bulk modulus becomes relatively greater than the shear modulus, with $K_\infty^u/G_\infty^u \simeq 35/3$ for $n = 4$. This indicates that the system becomes more "rubbery", certainly in terms of its high frequency response. Poisson's ratio ($\nu$) is about 0.5 for rubber and as (at zero frequency) the bulk, $K_0$ and shear $G_0$ moduli are related to Poisson's ratio via $K_0 = 2G_0(1+\nu)/(1-2\nu)$ for an isotropic solid (see e.g. [1]), then in the rubbery limit $K_0 \gg G_0$. Auxetic behaviour arises when $G_0 \gg K_0$. Of course for a liquid, $G_0 = 0$ so it is not meaningful to discuss an equilibrium (i.e. zero frequency response) Poisson's ratio, or whether any response is rubbery, auxetic or not.

In the hard sphere limit, we can obtain relatively simple and accurate expressions for $K_\infty$ and $G_\infty$ in terms of the hard sphere equation of state, [27,29],

$$G_\infty - \rho k_B T = \frac{1}{5}(P_{HS} - \rho k_B T)(n-3) + O(1), \quad (17)$$

or

$$\frac{G_\infty}{\rho k_B T} - 1 = \frac{1}{5}(Z_{HS}-1)(n-3) + O(1). \quad (18)$$

In the bulk modulus case, we have,

$$K_\infty - \frac{5}{3}\rho k_B T = \frac{1}{3}(P_{HS} - \rho_B T)(n+3) + O(1), \quad (19)$$

or [27,29],

$$\frac{K_\infty}{\rho k_B T} - \frac{5}{3} = \frac{1}{3}(Z_{HS}-1)(n+3) + O(1). \quad (20)$$

### 2.3 Self-diffusion coefficient

The self-diffusion coefficient is determined from the time dependence of the particle velocity,

$$D = \frac{1}{3}\int_0^\infty \langle \underline{v}(s+t)\cdot\underline{v}(s)\rangle_s \,\mathrm{d}t \quad (21)$$

where $\underline{v}$ is the velocity of the molecule, and the average is implicitly taken over the $N$ molecules in the system. It is useful to define a normalised velocity time correlation function as

$$\mathrm{C}_v(t) \equiv \frac{\langle \underline{v}(s+t)\cdot\underline{v}(s)\rangle_s}{\langle v^2(s)\rangle_s}, \quad (22)$$

so that this function has the convenient attribute of being dimensionless and having $C_v(0) = 1$. We also define an associated correlation time as,

$$\tau_v \equiv \int_0^\infty C_v(t)\,\mathrm{d}t, \quad (23)$$

so that from equations (21) to (22) we have,

$$D = \frac{k_B T}{m}\tau_v, \quad (24)$$

where $m$ is the mass of the molecule. See [16] for a discussion of the $n$-dependence of the velocity auto-correlation function and the self-diffusion coefficient.

### 2.4 Analysis of transport coefficient data

There are many semi-empirical formulae in the literature that express the transport coefficients of liquids in terms of a measurable property or order parameter (structural, density dependent) or thermodynamic. We consider a procedure, dating back to Batschinski [30] and Hildebrand, [31,32] to analyze the transport coefficients.

The diffusion coefficient $D$ and inverse shear viscosity $\eta_s^{-1}$, ("fluidity") of simple liquids were found to be linearly dependent on the molar volume $V$, at high liquid densities [31,32]. Thus $D = AV - B$ or $\eta_s^{-1} = AV - B$ where $A$ and $B$ are constants to be determined for each molecular system and transport coefficient. A more extensive study of the transport coefficients of simple molecular systems was carried out by van Loef [33,34], who demonstrated the accuracy of these formulas down to at least two thirds of the freezing density.

Although, real molecules can never be true hard spheres, the hard sphere reference system has been perhaps the main tool in developing thermodynamic and dynamical theories of the liquid state (e.g. [20], p. 146). The hard sphere simulation data at moderate to high densities can also be reproduced well by the Batschinski-Hildebrand treatment [35], which can be recast into a more convenient form for the present purposes, using the packing fraction, $\zeta_d = \pi d^3 N/6V$ rather than the molar volume. Let $\zeta_{d,i}$ be the value of the hard sphere packing fraction at which the transport coefficient (e.g. $D$) or its inverse (e.g. $\eta_s^{-1}$), on extrapolation with volume ($\propto \zeta_d^{-1}$), tends to zero.

$$\frac{D}{D^*} = \frac{1}{\zeta_d} - \frac{1}{\zeta_{d,i}}, \tag{25}$$

where $D$ is in units of $d(k_B T/m)^{1/2}$ and $d$ is again the hard sphere diameter. For the normalization constant, $D^* = 0.1408$ and $\zeta_{d,i} = 0.5350$ for $0.494 > \zeta_d > 0.370$ [35] or $0.923 > \zeta_d/\zeta_{d,i} > 0.692$. Sigurgiersson and Heyes, [36,37] based on their hard sphere simulation data and those of others, derived the revised values $D^* = 0.1222$ and $\zeta_{d,i} = 0.535$ (we use $\zeta_{d,i} = 0.5375$ in this work) for $0.519 > \zeta_d > 0.260$ or $0.952 > \zeta_d/\zeta_{d,i} > 0.476$ [36,37]. Similarly for the shear viscosity, $\eta_s$, in units of $d^{-2}(mk_B T)^{1/2}$,

$$\frac{\eta_s^*}{\eta_s} = \frac{1}{\zeta_d} - \frac{1}{\zeta_{d,i}}, \tag{26}$$

where $\eta_s^* = 1.0848$ and $\zeta_{d,i} = 0.5350$ for $0.494 > \zeta_d > 0.247$ or $2.166 > \zeta_{d,i}/\zeta_d > 1.083$.

In order to apply this treatment of the hard sphere to real (albeit "simple") molecules we require an effective hard sphere diameter $\sigma_{HS}$ for the real molecule. We have shown in ref. [38] that this analysis can be adapted and applied to much softer particles, in which an effective hard sphere diameter is implicitly assigned. Further developments of this treatement will be discussed in the "Results and discussion" section.

## 3. Simulation details

We have carried out MD simulations on the inverse power potential fluids to explore the behaviour of its various physical properties in the $n \to \infty$ (hard sphere) and very soft $n \to 4$ limits. Equilibrium MD simulations were carried out at $k_B T/\epsilon = 1$ on the potential of equation (1) with $n$ values ranging from 4 to 1152 on $N = 500$ and 864 particle systems. $n = 4$ is the maximum possible integer value of the exponent, as the various integrals defining static properties (e.g. energy per particle defined in equation (3)) do not converge for $n = 3$ and lower values. (Charged systems have $n < 3$, of course, but convergence there is ensured by charge cancellation at long range.) The simulations were carried out for typically 5–100 million timesteps down to $0.00008\sigma(m/\epsilon)^{1/2}$ for 1152. For $n = 4$, the simulations were for typically 2 million timesteps of 0.0075. For the large $n$ values, neighbour lists were implemented to reduce computer time, with an interaction cut-off, $r_c$, in each case based on the energy criterion $\phi(r_c) = k_B T\theta$ where $\theta = 10^{-4}$, which gives, $r_c/\sigma = (\epsilon/k_B T\theta)^{1/n}$. For $n = 4$ there was no point in implementing neighbour lists, as for the $N$ values considered, the interaction cut-off was close to or at half the simulation cell sidelength. Nevertheless, even for $N = 500$ and the highest packing fraction of 3.1 considered, this was possible. In this case, the cut-off was $r = 2.19\sigma$ and the corresponding interaction energy is $0.043k_B T$, which being significantly less than $k_B T$ was considered acceptable. The various transport coefficients were calculated by the Green-Kubo time correlation function route (supported also by simulations carried out with $N = 864$). For further details, see [12] for the self-diffusion coefficient and shear viscosity, [14] for the bulk viscosity and [15] for the thermal conductivity. In ths discussion, tables and figures, all quantities are expressed in terms of the usual reduced (pair potential) units $\sigma$ for length, $m$, the mass of the particle, for mass, and $\epsilon$ for energy. The simulations were carried out at $T^* = k_B T/\epsilon = 1$, and hence the quantities are also the same as the ~ones discussed in the previous section.

## 4. Results and discussion

Some of the key properties of the $r^{-n}$ fluids, including the energy particle $u$ and the transport coefficients are given in tables 1–5, for $n = 4, 6, 12, 18$ and 36, respectively. In figure 1, we show a plot of $D^{-1}$ against particle packing fraction, $\zeta = \pi N\sigma^3/6V$ for $N$ particles in volume $V$ for various values of $n$, and the $\sigma$ is that given in equation (1). $D^{-1}$ progressively increases more rapidly with particle packing fraction. The figure also shows that $D^{-1}$ decreases with smaller $n$ at a given value of $\zeta$. For large $n$, the data converge towards a common "hard sphere" line as the fluid in that limit tends to the hard sphere fluid itself, so that $\sigma$ and $d$ approach the same numerical value. Figure 2 shows a plot of the shear viscosity, $\eta_s$, against $\zeta$ for various values of $n$. As for the self-diffusion coefficient, for $n$ higher than about 72, the shear viscosity is statistically indistinguishable from that of hard spheres. For reference to help interpret the states on the figure, the phase diagram of the soft sphere system has been mapped out by Agrawal and Kofke [39]. The co-existence fluid

Table 1. Properties are shown of the $r^{-4}$ fluids from MD simulations carried out at $T^* = 1.0$ over a range of nominal packing fractions, $\zeta = (\pi N/6V)\sigma^3$.

| $\zeta$ | $u$ | $D$ | $\eta_s$ | $\eta_b$ | $\lambda$ |
|---|---|---|---|---|---|
| 1.00 | 20.411 | 0.136 | 1.27 | 0.310 | 6.88 |
| 1.20 | 25.746 | 0.103 | 1.56 | 0.283 | 9.43 |
| 1.35 | 29.934 | 0.0864 | 2.00 | 0.364 | 11.63 |
| 1.60 | 37.237 | 0.0659 | 3.22 | 0.431 | 15.25 |
| 1.85 | 44.906 | 0.0501 | 3.96 | 0.480 | 17.63 |
| 2.00 | 49.671 | 0.0432 | 5.21 | 0.585 | 21.43 |
| 2.00 | 49.672 | 0.0429 | 5.22 | 0.548 | 22.32 |
| 2.10 | 52.912 | 0.0391 | 6.10 | 0.645 | 25.53 |
| 2.20 | 56.203 | 0.0354 | 6.82 | 0.653 | 24.41 |
| 2.35 | 61.228 | 0.0310 | 7.84 | 0.742 | 28.44 |
| 2.50 | 66.355 | 0.0267 | 9.87 | 0.917 | 31.20 |
| 2.70 | 73.349 | 0.0219 | 10.91 | 1.14 | 34.20 |
| 2.70 | 73.348 | 0.0218 | 11.27 | 1.00 | 35.44 |
| 2.80 | 76.908 | 0.0197 | 11.67 | 1.00 | 33.79 |
| 2.90 | 80.508 | 0.0180 | 14.58 | 1.15 | 38.46 |
| 2.90 | 80.508 | 0.0180 | 13.35 | 1.28 | 40.43 |
| 3.10 | 87.829 | 0.0145 | 18.73 | 1.51 | 44.37 |
| 3.10 | 87.830 | 0.0148 | 18.74 | 1.50 | 40.11 |
| $\rho$* | | | | | |
| 0.60* | 10.734 | 0.254 | 0.61 | 0.155 | 3.15 |
| 0.80* | 15.391 | 0.184 | 0.89 | 0.191 | 5.45 |
| 1.50* | 34.269 | 0.0749 | 2.61 | 0.423 | 14.72 |
| 1.90* | 46.479 | 0.0488 | 4.60 | 0.544 | 19.58 |
| 2.20* | 56.196 | 0.0362 | 6.41 | 0.696 | 26.38 |
| 2.50* | 66.344 | 0.0270 | 9.24 | 0.893 | 30.40 |
| 2.65* | 71.569 | 0.0234 | 11.18 | 1.04 | 33.35 |
| 3.10* | 87.805 | 0.0151 | 18.69 | 1.67 | 45.08 |
| 3.10* | 87.805 | 0.0151 | 18.59 | 1.67 | 45.58 |

$u$ is the average potential energy per particle from equation (2); $D$ is the self-diffusion coefficient from equation (21); $\eta_s$ is the shear viscosity; $\eta_b$ is the bulk viscosity and $\lambda$ is the thermal conductivity from the appropriate Green-Kubo formulae. The number of particles employed in the the simulations was $N = 500$, except for the rows marked with * where $N = 864$ was used. Statistical uncertainties for this and subsequent tables are less than *ca.* 0.1% for $u$, ~1.0% for $D$ and 3–5% for $\eta_s$, $\eta_b$ and $\lambda$.



packing fractions are (with the $n$ values in brackets), for the thermodynamically stable bcc solid co-existing phase (from table 2 in [39]) 3.00(4) and 1.217(6) and for an fcc solid co-existing phase (from table 1 in [39]), 0.827(8), 0.611(12), 0.532(18) and 0.493(36).

We have replotted this data in the Batschinski-Hildebrand form in figures 3 and 4, which show plots of the normalized transport coefficient, $X(n, \zeta)$, where "$X$" denotes $D$ and $\eta_s^{-1}$, against $\zeta^{-1}$. Figure 3 shows that $D$ varies linearly with $\zeta^{-1}$ to a very good approximation for all $n$ studied. As for the hard spheres, there is a packing fraction $\zeta_i$ at which $D$ on extrapolation with volume ($\propto\zeta^{-1}$), is zero. There is a different line for each value of the potential exponent $n$, although they are more or less parallel. As $n$ decreases, $\zeta_i$, goes to higher packing fraction. In other words, the particles must be compressed to higher densities to obtain the same value for the transport coefficient, which is consistent with the trends in figures 1 and 2. One could view this as a decrease in the effective hard sphere diameter with increasing potential softness, although here we will not be considering this quantity explicitly. This linear trend allows us to draw a similarity with the behaviour of hard spheres, as embodied in equations (25) and (26), to obtain explicit formulas for the soft spheres. Inspection of figures 3 and 4 reveals the linear region extends to slightly higher packing fractions for the self-diffusion coefficient when compared with the shear viscosity (the higher packing fraction data points lie noticeably above the line). In fact, this linearity applies

Table 2. As for table 1, except that $n = 6$ and $N = 500$.

| $\zeta$ | $u$ | $D$ | $\eta_s$ | $\eta_b$ | $\lambda$ |
|---|---|---|---|---|---|
| 0.2086 | 1.202 | 0.534 | 0.245 | 0.0561 | 1.19 |
| 0.3000 | 2.044 | 0.377 | 0.351 | 0.149 | 2.07 |
| 0.4500 | 3.818 | 0.217 | 0.520 | 0.247 | 3.38 |
| 0.5000 | 4.538 | 0.183 | 0.754 | 0.301 | 4.00 |
| 0.5714 | 5.674 | 0.145 | 0.995 | 0.344 | 5.21 |
| 0.6000 | 6.164 | 0.141 | 1.025 | 0.425 | 5.64 |
| 0.6500 | 7.069 | 0.117 | 1.267 | 0.456 | 6.81 |
| 0.7000 | 8.034 | 0.0975 | 1.583 | 0.473 | 7.61 |
| 0.7500 | 9.062 | 0.0870 | 1.802 | 0.514 | 8.88 |
| 0.7900 | 9.928 | 0.0745 | 2.111 | 0.557 | 9.56 |
| 0.8600 | 11.540 | 0.0587 | 2.684 | 0.592 | 11.01 |
| 0.9000 | 12.515 | 0.0539 | 3.062 | 0.701 | 12.16 |
| 0.9900 | 14.855 | 0.0408 | 4.416 | 0.886 | 14.58 |
| 0.9900 | 14.856 | 0.0409 | 4.332 | 0.904 | 14.31 |
| 1.1100 | 18.289 | 0.0278 | 6.724 | 1.25 | 17.88 |
| 1.2500 | 22.749 | 0.0174 | 11.51 | 2.44 | 21.38 |

Table 3. As for table 1, except that $n = 12$ and $N = 500$.

| $\zeta$ | $u$ | $D$ | $\eta_s$ | $\eta_b$ | $\lambda$ |
|---|---|---|---|---|---|
| 0.1500 | 0.164 | 1.028 | 0.194 | 0.0306 | – |
| 0.1701 | 0.345 | 0.548 | 0.245 | 0.0980 | 1.156 |
| 0.2000 | 0.445 | 0.446 | 0.285 | 0.1334 | – |
| 0.2200 | 0.521 | 0.418 | 0.339 | 0.158 | 1.32 |
| 0.2551 | 0.674 | 0.323 | 0.384 | 0.228 | – |
| 0.2900 | 0.856 | 0.268 | 0.490 | 0.271 | 2.19 |
| 0.3500 | 1.247 | 0.180 | 0.667 | 0.470 | – |
| 0.3826 | 1.510 | 0.148 | 0.856 | 0.564 | 4.01 |
| 0.4000 | 1.667 | 0.132 | 0.949 | 0.619 | 4.34 |
| 0.4000 | 1.667 | 0.136 | 0.887 | 0.646 | 4.51 |
| 0.4250 | 1.914 | 0.117 | 1.137 | 0.690 | 5.08 |
| 0.4900 | 2.697 | 0.0715 | 1.959 | 1.089 | 7.07 |
| 0.5100 | 2.984 | 0.0640 | 2.369 | 1.428 | 7.68 |
| 0.5500 | 3.630 | 0.0440 | 3.312 | 1.652 | 9.19 |
| 0.5500 | 3.630 | 0.0442 | 3.389 | 1.681 | 9.19 |
| 0.5800 | 4.186 | 0.0332 | 4.685 | 2.307 | 10.56 |
| 0.6100 | 4.809 | 0.0258 | 6.395 | 3.212 | 11.77 |
| 0.6500 | 5.758 | 0.0151 | 11.67 | 7.366 | 13.55 |
| 0.6660 | 6.177 | 0.0120 | 16.79 | 8.364 | 14.46 |

Table 4. As for table 1, except that $n = 18$ and $N = 500$.

| $\zeta$ | $u$ | $D$ | $\eta_s$ | $\eta_b$ | $\lambda$ |
|---|---|---|---|---|---|
| 0.1819 | 0.236 | 0.476 | 0.277 | 0.130 | – |
| 0.2729 | 0.481 | 0.256 | 0.484 | 0.345 | 2.22 |
| 0.3000 | 0.583 | 0.212 | 0.541 | 0.460 | 2.68 |
| 0.3300 | 0.714 | 0.176 | 0.713 | 0.571 | 3.11 |
| 0.3600 | 0.871 | 0.142 | 0.892 | 0.655 | 3.86 |
| 0.4093 | 1.194 | 0.0950 | 1.388 | 1.023 | 5.31 |
| 0.4350 | 1.401 | 0.0756 | 1.748 | 1.387 | 6.19 |
| 0.4500 | 1.538 | 0.0659 | 2.094 | 1.393 | 7.01 |
| 0.4650 | 1.685 | 0.0575 | 2.541 | 1.659 | 7.88 |
| 0.4750 | 1.791 | 0.0525 | 2.910 | 2.079 | – |
| 0.4850 | 1.903 | 0.0464 | 2.945 | 2.062 | 8.74 |
| 0.4950 | 2.022 | 0.0409 | 3.634 | 2.570 | – |
| 0.5050 | 2.147 | 0.0361 | 4.152 | 2.919 | 9.15 |
| 0.5100 | 2.212 | 0.0342 | 4.345 | 3.957 | – |
| 0.5250 | 2.420 | 0.0278 | 5.337 | 4.309 | 10.44 |
| 0.5450 | 2.727 | 0.0206 | 7.921 | 5.497 | 11.50 |
| 0.5750 | 3.258 | 0.0117 | 14.12 | 14.87 | 12.27 |

Table 5. As for table 1, except that $n = 36$ and $N = 500$.

| $\zeta$ | $u$ | $D$ | $\eta_s$ | $\eta_b$ | $\lambda$ |
|---|---|---|---|---|---|
| 0.1903 | 0.117 | 0.423 | 0.317 | 0.166 | 1.44 |
| 0.2854 | 0.245 | 0.217 | 0.590 | 0.499 | 2.64 |
| 0.4281 | 0.662 | 0.0631 | 2.188 | 2.007 | 7.21 |
| 0.4500 | 0.770 | 0.0487 | 2.874 | 2.700 | 8.25 |
| 0.4800 | 0.948 | 0.0312 | 4.515 | 4.963 | 10.11 |
| 0.4940 | 1.046 | 0.0245 | 6.252 | 6.647 | 10.99 |
| 0.5100 | 1.172 | 0.0176 | 8.794 | 10.93 | 11.74 |

only in an "intermediate" density regime, between the dilute gas and the "glassy" states, which is nevertheless important as many systems of interest fall within this region.

The straight lines through the MD points on figures 3 and 4 are linear regression fits to the data using the equation,

$$X(n, \zeta) = a(n)\frac{1}{\zeta} - b(n), \tag{27}$$

where $b(n) = a(n)/\zeta_i(n)$, which is the Batschinski-Hildebrand formula for the generic transport coefficient, $X$, written in terms of the packing fraction $\zeta$ rather than the molar volume $V$. We have chosen

$$a(n) = a_0 + a_1 n^{-1} + a_2 n^{-2} + a_3 n^{-3}, \tag{28}$$

and

$$b(n) = b_0 + b_1 n^{-1} + b_2 n^{-2} + b_3 n^{-3}, \tag{29}$$

which fits the simulation data well. The terms $a_0$ and $b_0$ are respectively $a$ and $b$ in the hard sphere limit, whose values we already know, as discussed together with equations (25) and (26) Returning to equations (25) and (26) we can see that for self-diffusion, $a_0 = D^*$ and $b_0 = D^*/\zeta_{d,i}$, where $\zeta_{d,i} = 0.5375$. For shear viscosity, these limiting values are, $a_0 = 1/\eta_s^*$ and $b_0 = 1/\eta_s^*\zeta_{d,i}$, with $\zeta_{d,i} = 0.5350$, respectively.

The formulas in equations (28) and (29) are consistent with the trend that in the hard sphere (infinite $n$) limit the soft system can be assumed to behave as a hard sphere fluid with an effective hard sphere diameter (i.e. $d$) which in this limit is also equal to $\sigma$. In fact, the hard sphere units become identical to the soft sphere reduced units for infinite $n$. The linear regression analysis of the simulation data gives the analytic function parameters $a(n)$ and $b(n)$ for each transport coefficient. We have chosen to emphasise the small $n$ region in fitting the parameters, $a_1, a_2$ and $a_3$ and $b_1, b_2$ and $b_3$. The least squares fit parameters from equations (28) and (29) are given in the captions to figures 3 and 4 for the two transport coefficients. The agreement of the MD data and the formula in equation (27) is generally very good in the intermediate density region, but at the highest packing fractions the formula overestimates the viscosity and underestimates the self-diffusion coefficient. This is consistent with the very lowest data points on figures 1 and 2 being a little above the best fit lines.

We now turn to other properties of the soft-sphere systems where we seek further elucidation of the mechanical and rheological behaviour. Because of a presumed enhanced "connectivity" within the softer systems one might expect fluctuations in ensemble average properties to decrease in the soft particle ("rubbery") limit. This should be manifest in the pressure fluctuations which are conveniently expressed

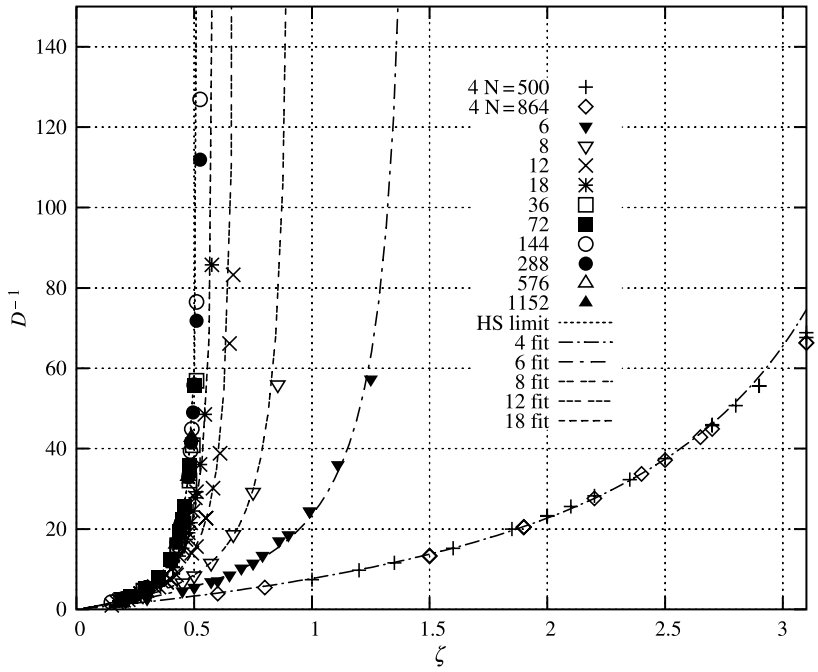


Figure 1. Plot of the inverse self-diffusion coefficient, $D^{-1}$ against the packing fraction $\zeta = \pi N\sigma^3/6V$ for various $n$ values. $D$ is in units of $\sigma(\epsilon/m)^{1/2}$ where $\sigma$ and $\epsilon$ are the potential parameters from equation (1). The dashed line ("HS limit") is meant to guide the eye for the limiting case of hard sphere behavior. The other curves are the predictions of the fit formula of equation (27), where $X \equiv D$ with the fit parameters for $a(n)$ of equation (28) and $b(n)$ of equation (29) given in the caption of figure 3.

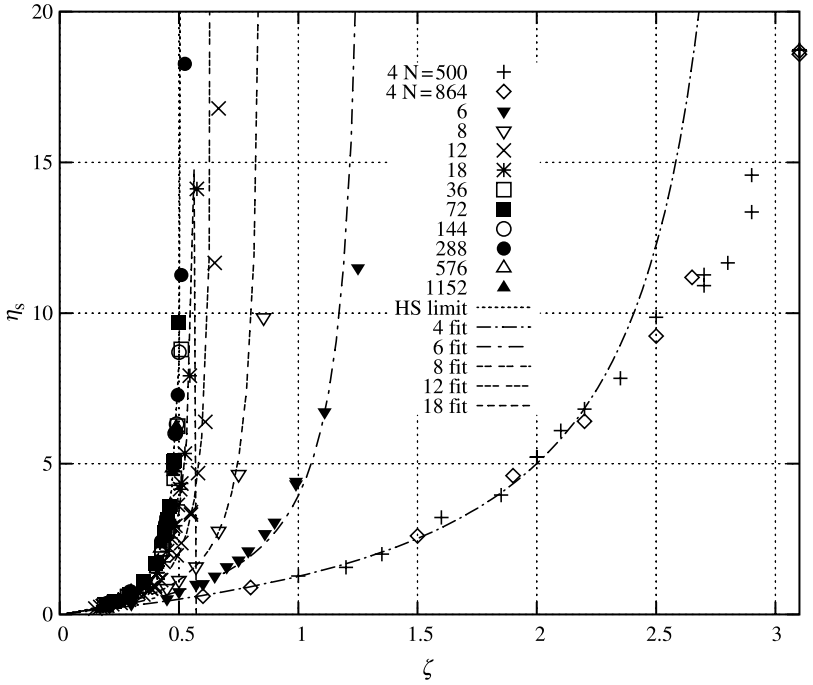


Figure 2. As for figure 1, but with the shear viscosity, $\eta_s$ plotted against the packing fraction for various values of $n$. $\eta_s$ is in units of $\sigma^{-2}(m\epsilon)^{1/2}$ where $\sigma$ and $\epsilon$ are the potential parameters from equation (1). The other curves are the predictions of the fit formula of equation (27), where $X \equiv \eta_s^{-1}$, with the parameters for $a(n)$ and $b(n)$ given in the caption of figure 4.



(by eliminating the formal $N$-dependence) in terms of the difference between the infinite and zero frequency bulk moduli, $K_\infty - K_0 = (V/k_BT)\langle(\delta P)^2\rangle$ where $\delta P = P - \langle P\rangle$ and $\langle\cdots\rangle$ again denotes a time average. Figure 5 shows this quantity as a function of $\zeta$ for various $n$ values. The data points for each $n$ terminate close to the co-existence fluid packing fraction. One can see that the pressure fluctuations systematically decrease with diminishing $n$ value for corresponding packing fractions on the phase diagram. This figure also suggests that for very soft particles $K_\infty \simeq K_0$, i.e. the zero and infinite frequency bulk moduli are similar an magnitude. This can be seen more

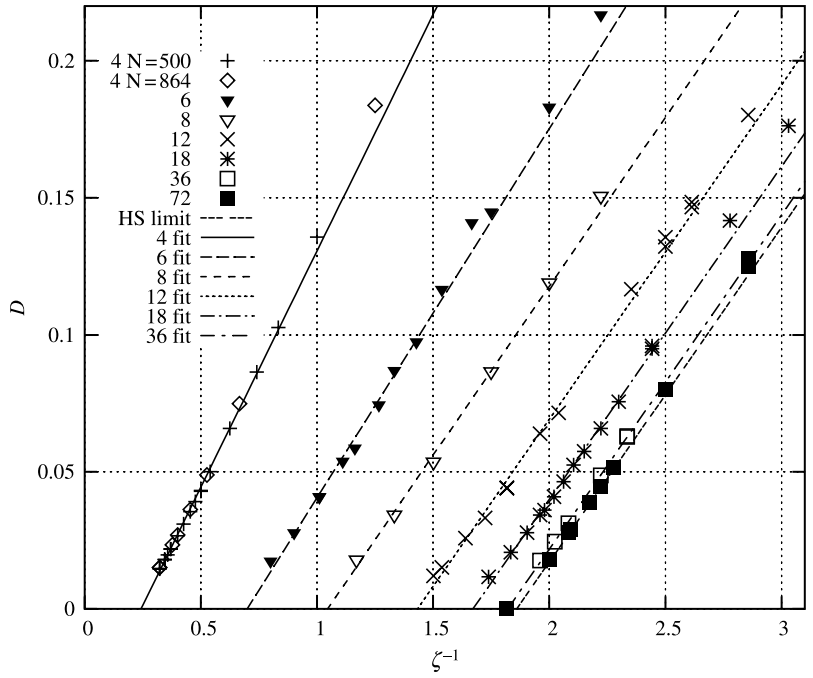


Figure 3. $D$ against $\zeta^{-1}$ where $D$ is in units of $\sigma(\epsilon/m)^{1/2}$. The straight lines are least square fits to the diffusion coefficient data in the range $D < 0.1222$, using the fit formula of equation (27), where $X \equiv D$. The slopes $a(n)$ and intercepts $b(n)$ were least squares fitted to the simple analytic expressions given in equations (28) and (29), respectively. This gave, $a_0 = 0.1222, a_1 = -0.026170, a_2 = -0.11616$ and $a_3 = 4.10694$, and $b_0 = 0.227349, b_1 = -0.140798, b_2 = -7.388764$ and $b_3 = 19.96254$.

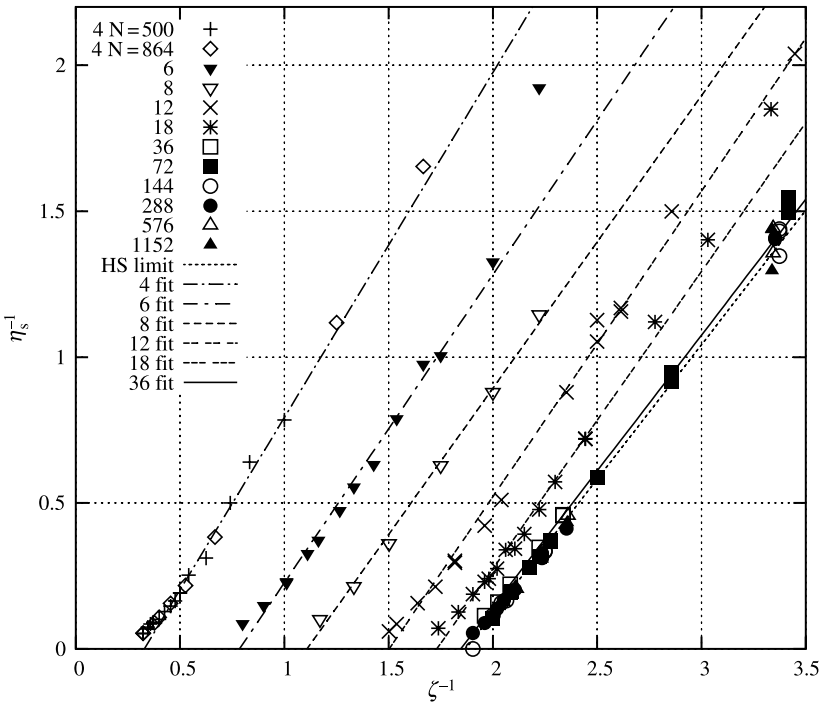


Figure 4. $\eta_s^{-1}$ against $\zeta^{-1}$, in units of $\sigma^{-2}(m\epsilon)^{1/2}$. The straight lines are least square fits to the inverse shear viscosity data in the range $\eta_s^{-1} < 1.3827$, using the fit formula of equation (27), where $X \equiv \eta_s^{-1}$. The slopes $a(n)$ and intercepts $b(n)$ were fitted to the simple analytic expressions given in equations (28) and (29), respectively. This gave, $a_0 = 0.921829, a_1 = 2.26136, a_2 = -17.354972$ and $a_3 = 49.861825$ and $b_0 = 1.72304, b_1 = 4.892204, b_2 = -106.64916$ and $b_3 = 263.0707$.

conclusively in figure 6 which shows the ratio, $(K_\infty - K_0)/K_\infty$. For the very soft particles, this ratio is $\ll 1$, for the softer systems at higher packing fractions, which confirms that in this limit, $K_\infty \simeq K_0$. Hence, the frequency dependence of the bulk modulus is relatively weak for the very soft particles.

Are there any fundamental structural differences between the large $n$ systems (say, $n \geq 12$) and those with smaller $n$? The following discussion is meant to provide some initial pointers, from this pilot study, without claiming to be definitive. Figure 7 shows the position of the first peak $r_{max}$ and first minimum

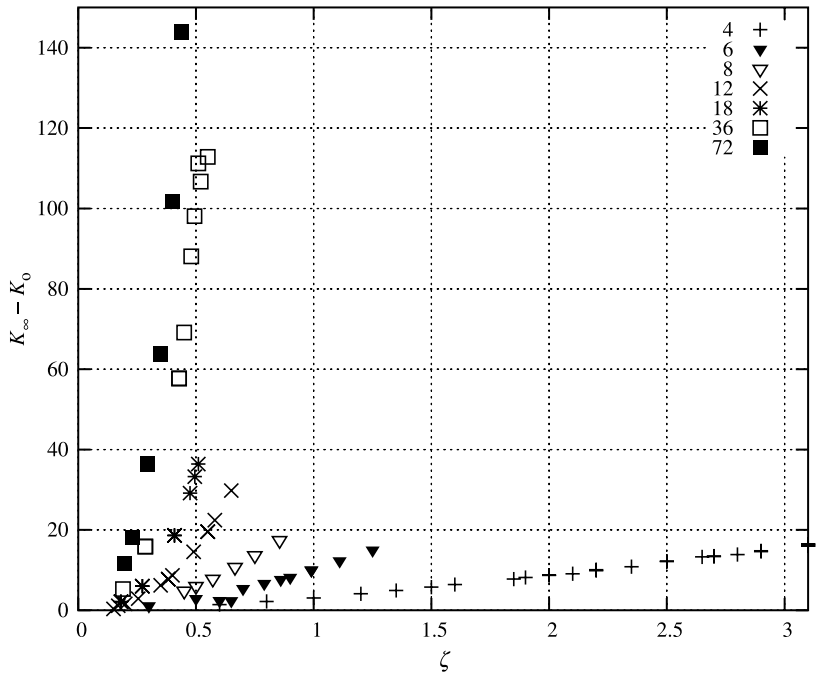


Figure 5. $K_\infty - K_0$ against $\zeta$ for various packing fractions and $n$ (indicated in the figure). This quantity is calculated from the average square of the deviation in the pressure about the mean, i.e. $K_\infty - K_0 = (V/k_BT)\langle(P - \langle P\rangle)^2\rangle$.

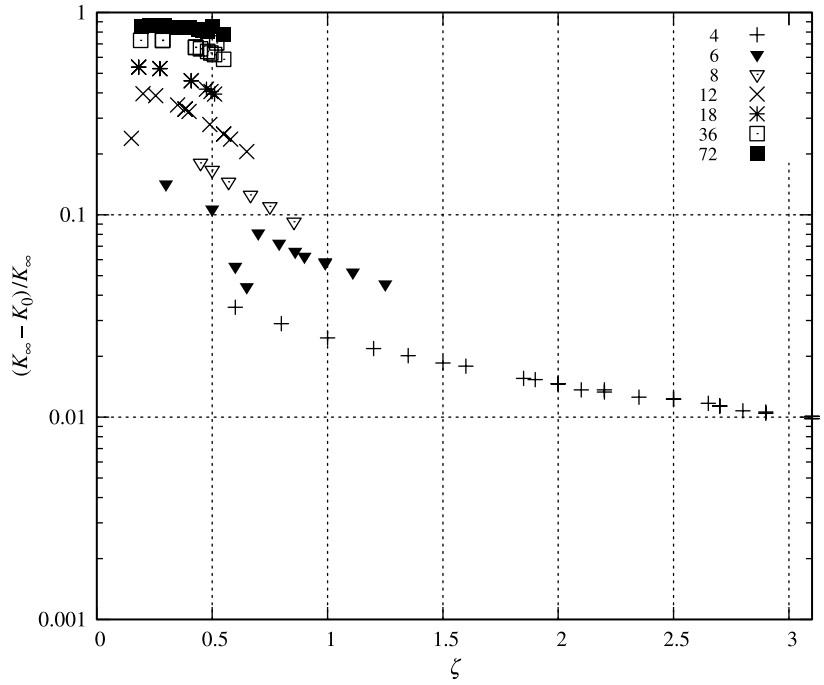


Figure 6. $(K_\infty - K_0)/K_\infty$ against $\zeta$ for various packing fractions and $n$ (indicated on the figure). To calculate this ratio we obtain the numerator as for figure 5, and the denominator from equation (16).



$r_{\min}$, in the radial distribution function as a function of packing fraction. There is a monotonic decrease with $\zeta$ in both cases. One might expect that in the soft particle limit, a mean field treatment might successfully account for $r_{\max}$, with the ideal gas becoming the new reference state (rather than the hard sphere which is used for $n \to \infty$). If one assumes a random distribution of points and that $r_{\max} \simeq 1$ at the hard sphere glass transition ($\zeta = 0.58$ [40]) we have $r_{\max} \simeq (0.58/\zeta)^{1/3}$, which is plotted in the figure. This formula (marked "MF" on the figure) goes through the simulation data quite well for the very soft particles but not for the extremely hard ones which have a maximum fluid packing fraction of *ca.* 0.5. There is a gradual transition between the two extremes of behaviour. Figure 8 shows the corresponding values of the first maxima and minima in $g(r)$. There is a systematic trend in the values of these

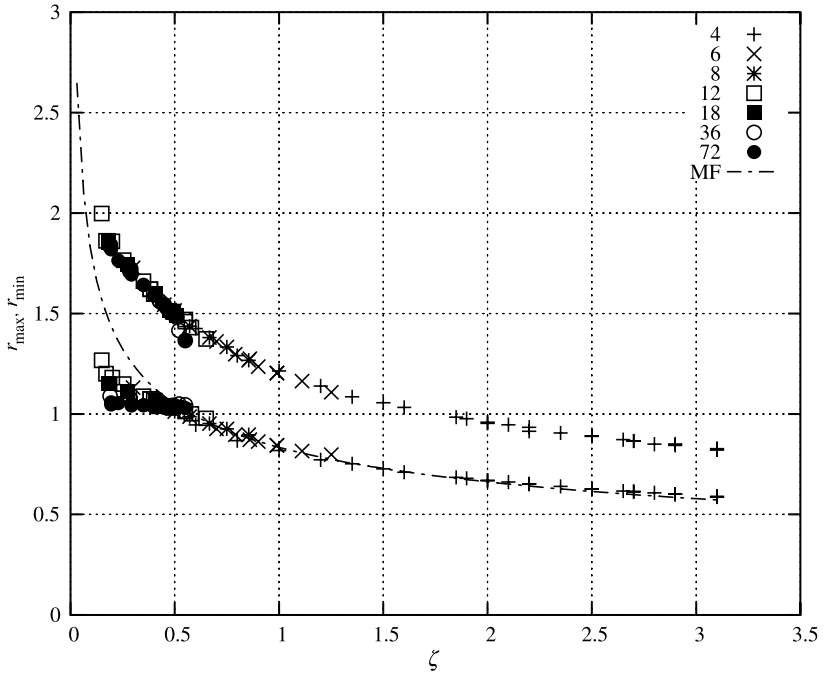


Figure 7. Lower set of data is $r_{\max}$, the position of the first maximum in $g(r)$, against $\zeta$ for various $n$ which are given in the figure. The upper set of data is $r_{\min}$, the position of the first minimum in $g(r)$. The continuous curve ("MF") is $(0.58/\zeta)^{1/3}$.

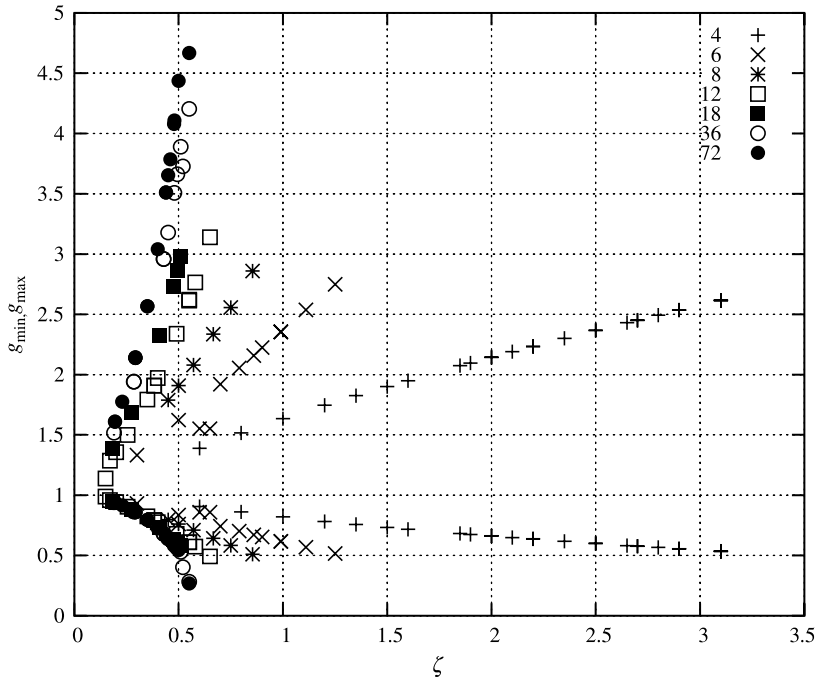


Figure 8. Upper set of data is $g(r)_{max}$, the value of the first maximum in $g(r)$, against $\zeta$ for various $n$. The lower set of data is $g(r)_{min}$, the value of the first minimum in $g(r)$.



two quantities with softness and packing fraction. The first maximum increases in height with packing fraction while the first minimim decreases in height. The value of $g(r_{max})$ is $\simeq 2.6$ for the fluid at co-existence for $n \leq 12$, but increases to 5.8 for hard spheres (using the Carnahan-Starling prediction $g_{max} = (1 - \zeta/2)(1 - \zeta)^{-3}$ and $\zeta = 0.494$ for the co-existence fluid packing fraction of hard spheres). Hansen and Verlet conjectured on the basis of there simulation data that the first peak in the structure factor of the fluid at freezing should be $\sim 2.8$ for a wide range of liquids [41].

Figure 9 shows the value of the coordination number $C_n$, as the integral of $g(r)$, evaluated up to the first peak $r_{max}$ and first minimum, $r_{min}$. The number of interacting

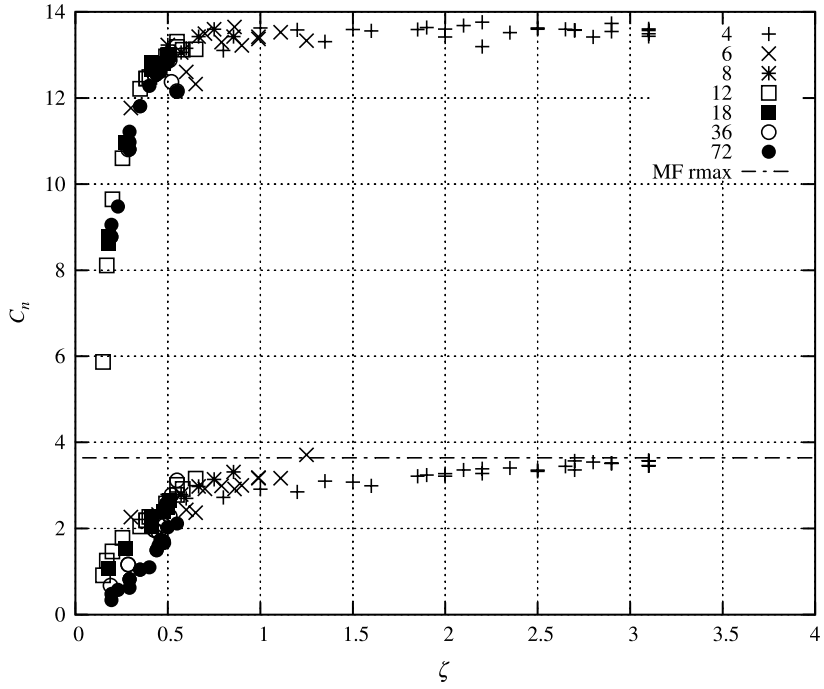


Figure 9. The coordination number, $C_n$ against $\zeta$ for various $n$ (indicated on the figure). Shown are the $C_n$ calculated from the radial distribution function up to the first maximum (lower set of data) and first minimum (upper set of data). The horizontal line at 3.64 is the mean field prediction ("MD rmax").

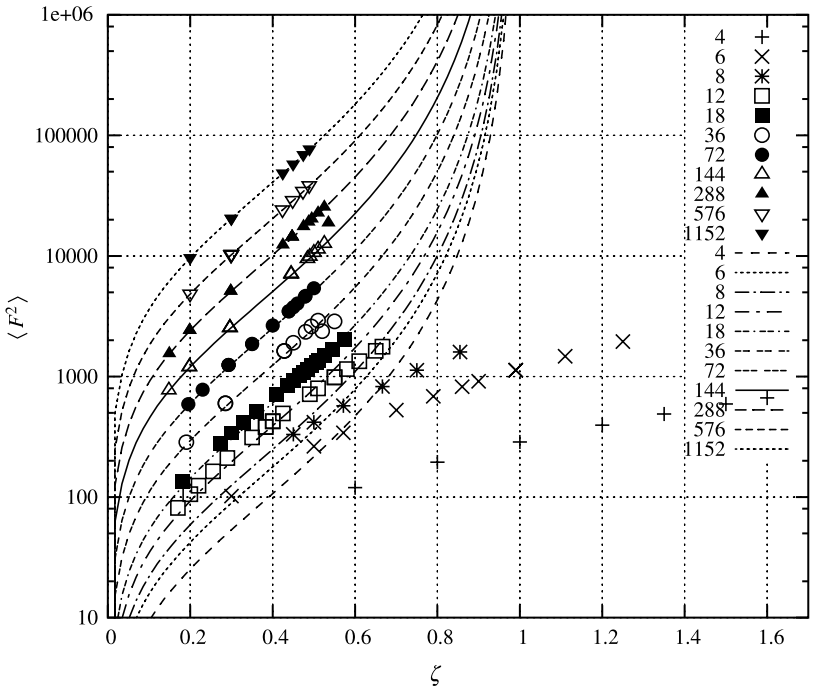


Figure 10. Plot of the mean square force, $\langle F^2 \rangle$ in the reduced units $\epsilon^2/\sigma^2$ against packing fraction, $\zeta = \pi N \sigma^3/6V$, for the potential given in equation (1). The lines are the predictions of the hard sphere perturbation theory given in equation (30).



neighbours within $r_{\min}$ increases up to a value of $\simeq 13$ at co-existence, as evident in figure 9. Note that for $n = 4$ there is a wide density range from *ca.* 1.0 to 3.0 where these two co-ordination numbers hardly change. There is some form of "self-correction" that takes place which accommodates the density change while maintaining a co-ordination number that hardly changes. The mean field ("MF") value of the co-ordination number up to a distance of $r_{\max}$ given in the figure is based on the simple criterion based on a uniform distribution of particles in a sphere of radius $r_{\max}$. This treatment yields, $C_n = 8\zeta r_{\max}^3 - 1$, (the "1" removes the particle at the origin), which gives $C_n = 8 \times 0.58 - 1 = 3.64$ (note the packing fraction dependence has disappeared). The variable$y = 3.64$ appears as a horizontal line in the figure, and it can be seen that the simulation data for the co-ordination number evaluated up to the first maximum in $g(r)$ converge towards this line for $\zeta \simeq 3.0$.

Figure 10 shows the mean square force $\langle F^2 \rangle$ on an arbitrary particle, for a range of $n$ values, given in the figure. The $\langle F^2 \rangle$ are numerically quite large and increase with the steepness of the potential. For example, for $n = 12$ close to the maximum fluid density this ratio is $\sim 1000$. In the $n \to \infty$ limit, an analytically accurate expression for this ratio is, [18]

$$\langle F^2 \rangle = \frac{6(k_B T)^2 m}{\sigma_{HS}^2}(n-1)(Z_{HS}-1) + O(1), \qquad (30)$$

where $\sigma_{HS}$ is an effective hard sphere diameter and $Z_{HS}$ is the compressibility factor of the hard sphere fluid. The analytic formula provided by Carnahan and Starling [22], for example, is adequate for the present (graphical) purposes, i.e.

$$Z_{HS} = (1 + \zeta_d + \zeta_d^2 - \zeta_d^3)/(1 - \zeta_d)^3. \qquad (31)$$

For the hard sphere fluid $\langle F^2 \rangle$ is of course infinite as can be seen from equation (30), physically because of the infinite forces experienced in the elastic hard sphere collisions. The lines on figure 10 are the predictions of equation (30) where we have simpe set $\sigma_{HS} = \sigma$ (the length parameter in the soft sphere potential). This is clearly a drastic simplification for small $n$ values, but in figure 9 this shows down to what values of $n$ this simple analytic prescription for the mean square force is applicable. The figure shows that the approximation is quite adequate down to *ca.* $n = 18$. For small values of $n$ the formula overpredicts the mean square force, at least in part, because the effective hard sphere diameter is in reality much less than $\sigma$, and there the hard sphere equation of state is probably not applicable within this range of parameter values.

It is informative to compare how the various transport coefficients vary with density and softness. For the self-diffusion coefficient and shear viscosity, the Stokes–Einstein relationship provides a natural framework for comparison (see, e.g. [20], p. 210). This gives $D\eta_s = k_B T/3\pi\sigma_{HS}$ for "stick" boundary conditions and $D\eta_s = k_B T/2\pi\sigma_{HS}$ for "slip" boundary conditions. Therefore, a plot of $2\pi\sigma_{HS} D\eta_s/k_B T$ should range from $2/3$ for stick to 1 for slip conditions. In figure 11, this quantity is plotted against packing fraction for various $n$ values. We have set $\sigma_{HS} = r_{\max}$ for this exercise. For not too small $n$, the ratio increases

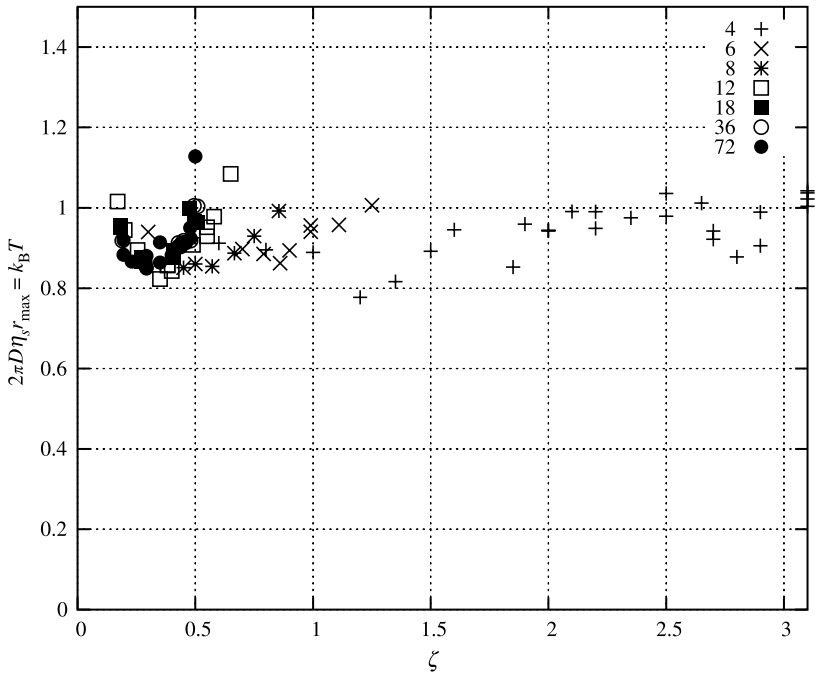


Figure 11. $2\pi D\eta_s r_{max}/k_B T$ against $\zeta$ for various $n$. $D$ is the self-diffusion coefficient, $\eta_s$ is the shear viscosity and $r_{max}$ is the position of the first peak in the radial distribution function. All three quantities are derived from the simulation results. The values of $n$ used are given in the figure.



towards the slip limit with increasing density. For very low and decreasing density, this ratio increases because $D$ is inversely proportional to density and $\eta_s$ is independent of density in the infinitely dilute limit as is well known from kinetic theory. The issue of softness does not appear to introduce any new qualitative trend or dependence here.

The bulk and shear viscosities are two quantities that are often compared. The density and $n$ dependence of the ratio $\eta_b/\eta_s$ is shown in figure 12. The figure shows that this ratio is typically less than 1 except perhaps for the highest packing fractions and steepest interactions. However, for the small $n$ values this ratio does decrease with increasing packing fraction, and is always below 1. So in this quantity there appears to be some qualitatively new trend for the very soft systems ($n < 12$). It is worth noting that although the bulk viscosity becomes much smaller than the shear viscosity for small $n$ and higher density, the reverse trend is manifest by the corresponding infinite frequency shear moduli. Figures 5 and 6 show that

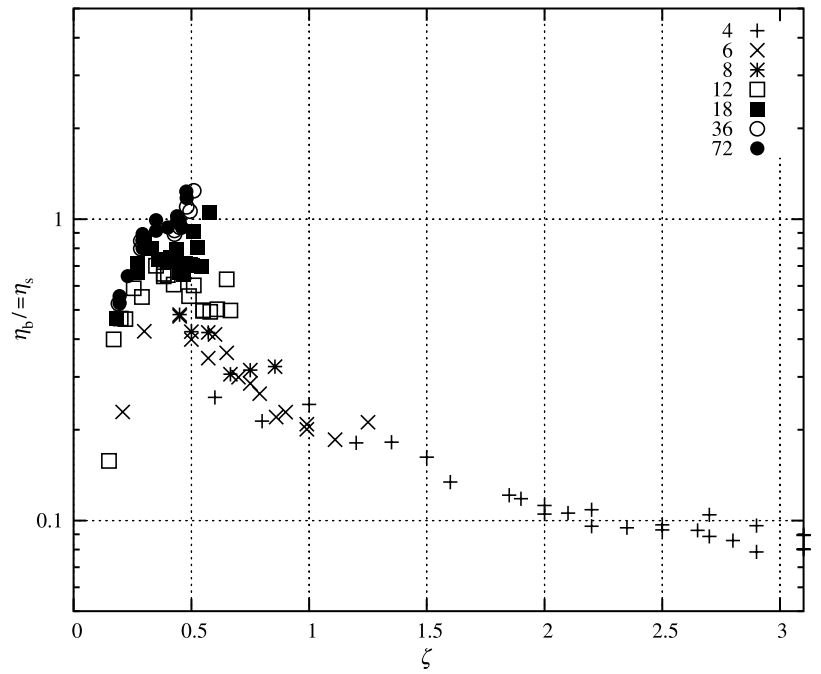


Figure 12. Plot of the ratio of the bulk to shear viscosity, $\eta_b/\eta_s$ against $\zeta$. The values of $n$ used are given in the figure.

$K_\infty - K_0$ are particularly small for the softer systems and higher densities, and much smaller than the $K_\infty$, which must be a significant factor in explaining the trend seen in figure 12.

## 5. Conclusions

Why do we think this study could be of relevance in understanding auxetic materials? The more coarse grained the representation of a material, often the softer the interaction becomes between the interacting units. For example, although auxetic materials are usually constructed from quite stiff members, on a larger lengthscale than these members the response to bulk deformation is quite soft, as the construction as a whole manifests a compliant response through cooperative movement of its members. This feature may allow us to develop coarse-grained models for such materials in which relatively soft simply shaped building units are deemed to interact with each other through a central force, or another relatively simple interaction form (possibly involving tangential components to represent rotational motion). It is, therefore, of interest to know how very soft repulsive-core particles interact in an assembly.

This study has extended our previous characterisation of soft sphere fluids (see in particular [38]) down to even softer particles, where the exponent ($n$) is only 4 (3 is the lowest value one can have for a thermodynamically defined system). Trends that were just appearing for $n = 6$ become much clearer and more pronounced for $n = 4$, which has an extremely wide fluid range up to a nominal packing fraction of 3.0 when compared with the value of 0.5 for hard spheres. The compressibility of these soft particles introduces a compliance in the structure, with the average separation between nearest neighbour particles and corresponding coordination number well described by a simple mean field expression. For all $n$ the coordination number up to the first minimum in the radial distribution function is about 13 for the highest density states close to coexistence with the solid. The value of 13 for $n = 4$ persists essentially from a nominal packing fraction of *ca.* 1.0 to 3.0. Therefore, the coordination number of 13 appears to be a relatively invariant feature of the soft sphere fluids for *all* $n$. This would support the conclusions of Ben-Amotz and Stell [10] that even for $n = 4$ some aspects of hard sphere perturbation theory can be retained and used to account for the local structure of these systems. For the very soft particles both the infinite and zero frequency bulk compressional moduli are of similar magnitude and rather high compared to the shear modulus behaviour, which is typical of a rubbery material.

The density dependence of the self-diffusion coefficient and shear viscosity satisfy the Batchinski–Hildebrand relationship, even for $n = 4$, which is quite different from the range of $n$ for which this formula was originally proposed and confirmed (i.e. simple molecules, where $n \simeq 12$).

To conclude, the auxetic materials behave in a way, i.e. the opposite to these soft particles. It would therefore cast doubt on our ability to represent auxeticity in terms of a soft effective interaction, at least of the central force variety. One requires a high shear modulus and a low bulk modulus and the current type of very soft particles give the opposite relative magnitude. In the infinite $n$ and infinite frequency limit, we are bounded by $K_\infty/G_\infty \simeq 5/3$. Our accompanying article in this Special Issue adopts a different conceptual approach, by simulating quite hard particles aimed at representing the individual rigid members in the body. In that case, we have a more detailed representation of the material, where trends towards producing an auxetic effect can be seen.

## Acknowledgements

The authors would like to thank Dr N. Gasper (University of Exeter, UK) for useful discussions. ACB and DMH thank the Royal Society (London) and the Polish Academy of Sciences for partly funding this collaboration. The work has been partially supported by the Polish Committee for Scientific Research (KBN) grant No. 4T11F01023.

## References

[1] R. Lakes. Foam structures with a negative Poisson's ratio. *Science*, **235**, 1038 (1987).
[2] B.D. Caddock, K. Evans. Microporous materials with negative Poisson's ratios. I. Microstructure and mechanical properties. *J. Phys. D*, **22**, 1877 (1987).
[3] D. Kang, M.P. Mahajan, S. Zhang, R.G. Petschek, C. Rosenblatt, C. He, P. Liu, A.C. Griffin. Pretransitional behavior above the nematic-isotropic phase transition of an auxetic trimer liquid crystal. *Phys. Rev. E*, **60**, 4980 (1999).
[4] K.E. Evans, A. Alderson. Auxetic materials: functional materials and structures from lateral thinking! *Adv. Mater.*, **12**, 617 (2000).
[5] K.E. Evans, M.A. Nkansah, I.J. Hutchinson, S.C. Rogers. Molecular network design. *Nature*, **353**, 124 (1991).
[6] A. Alderson, J. Rasburn, S. Ameer-Beg, P.G. Mullarkey, W. Perrie, K.E. Evans. An auxetic filter: a tuneable filter displaying enhanced size selectivity or defouling properties. *Ind. Eng. Chem. Res.*, **39**, 654 (2000).
[7] A. Spadoni, M. Ruzzene, F. Scarpa. Global and local linear buckling behavior of a chiral cellular structure. *Phys. Stat. Sol. B*, **242**, 695 (2005).
[8] A. Alderson, K.E. Evans. Molecular origin of auxetic behavior in tetrahedral framework silicates. *Phys. Rev. Lett.*, **89**, 225503 (2002).
[9] P.A. Langston, U. Tüzün, D.M. Heyes. Discrete element simulation of granular flow in 2D and 3D Hoppers: Dependence of discharge rate and wall stress on particle interactions. *Chem. Eng. Sci.*, **50**, 967 (1995).
[10] D. Bem-Amotz, G. Stell. Hard sphere perturbation theory for fluids with soft repulsive core potentials. *J. Chem. Phys.*, **120**, 4844 (2004).
[11] R. Agrawal, A.D. Kofke. Solid–fluid coexistence for inverse-power potentials. *Phys. Rev. Lett.*, **74**, 122 (1995).
[12] D.M. Heyes, J.G. Powles. Thermodynamic, mechanical and transport properties of fluids with steeply repulsive potentials. *Mol. Phys.*, **95**, 259 (1998).
[13] J.G. Powles, G. Rickayzen, D.M. Heyes. Purely viscous fluids. *Proc. Roy. Soc. Series A*, **455**, 3725 (1999).
[14] J.G. Powles, D.M. Heyes. Viscoelastic behaviour of fluids with steeply repulsive potentials. *Mol. Phys.*, **98**, 917 (2000).

[15] D.M. Heyes, J.G. Powles. Thermal conductivity of fluids with steeply repulsive potentials. *Mol. Phys.*, **99**, 1077 (2001).
[16] D.M. Heyes, J.G. Powles, G. Rickayzen. The velocity autocorrelation function and self-diffusion coefficient of fluids with steeply repulsive potentials. *Mol. Phys.*, **100**, 595 (2002).
[17] A.C. Brańka, D.M. Heyes. Time correlation functions of hard sphere and soft sphere fluids. *Phys. Rev. E.*, **69**, 021202 (2004).
[18] D.M. Heyes, G. Rickayzen, A.C. Brańka. Static properties and time correlation functions of fluids with steeply repulsive potentials. *Mol. Phys.*, **102**, 2057 (2004).
[19] A.C. Brańka, D.M. Heyes. The effects of particle softness on the dynamics of molecular and colloidal liquids. *Mol. Phys.*, **103**, 2359 (2005).
[20] J.-P. Hansen, I.R. McDonald, *Theory of Simple Liquids*, 2nd Ed., Chap. 6, p. 145, Academic Press, London (1986).
[21] A. Mulero, C. Galán, F. Cuadros. Equations of state of hard spheres. A review of accuracy and applications. *Phys. Chem. Chem. Phys.*, **3**, 4991 (2001).
[22] N.F. Carnahan, K.E. Starling. Equation of state of nonattracting rigid spheres. *J. Chem. Phys.*, **51**, 635 (1969).
[23] A.C. Brańka, D.M. Heyes. Elastic properties of inverse power fluids. *Comp. Methods Sci. Techn.*, **10**, 127 (2004).
[24] A.C. Brańka, D.M. Heyes. Equation of state of inverse power fluids. *Mol. Phys.*, **102**, 2049 (2004).
[25] A.C. Brańka, D.M. Heyes, to be submitted.
[26] J.C. Maxwell. On the dynamical theory of gases. *Phil. Trans. R. Soc.*, **157**, 49 (1867).
[27] G. Rickayzen, J.G. Powles, D.M. Heyes. Viscoelasticity of fluids with steeply repulsive potentials. *J. Chem. Phys.*, **118**, 11048 (2003).
[28] R.W. Zwanzig, R.D. Mountain. High-frequency elastic moduli of simple fluids. *J. Chem. Phys.*, **43**, 4464 (1965).
[29] D.M. Heyes. Thermodynamics and elastic moduli of fluids with steeply repulsive potentials. *J. Chem. Phys.*, **107**, 1963 (1997).
[30] A.J. Batschinski. Untersuchungen über die innere Reibung der Flüssigkeiten. *Z. Phys. Chem.*, **84**, 643 (1913).
[31] J.H. Hildebrand. Motions of molecules in liquids: viscosity and diffusivity. *Science*, **174**, 490 (1971).
[32] J.H. Hildebrand. *Viscosity and Diffusivity: A Predictive Approach*, John Wiley & Sons, New York (1986).
[33] J.J. van Loef. Temperature and volume dependence of transport properties of very dense van der Waals fluids. *Physica B*, **114**, 345 (1982).
[34] J.J. van Loef. Transport properties of dense monatomic and molecular fluids and their mixtures, and the corresponding states principle I. Shear viscosity and thermal conductivity. *Physica B*, **124**, 305 (1984).
[35] J.H. Dymond. Corrected Enskog Theory and the transport coefficients of liquids. *J. Chem. Phys.*, **60**, 969 (1974).
[36] H. Sigurgeirsson, D.M. Heyes. Transport coefficients of hard sphere fluids. *Mol. Phys.*, **101**, 469 (2003).
[37] D.M. Heyes, H. Sigurgeirsson. The Newtonian viscosity of concentrated stabilized dispersions: Comparisons with the hard sphere fluid. *J. Rheol.*, **48**, 223 (2004).
[38] D.M. Heyes, A.C. Brańka. The influence of potential softness on the transport coefficients of simple fluids. *J. Chem. Phys.*, **122**, 234504 (2005).
[39] R. Agrawal, D.A. Kofke. Thermodynamic and structural properties of model systems at solid-fluid coexistence I. Fcc and bcc soft spheres. *Mol. Phys.*, **85**, 23 (1995).
[40] R.J. Speedy. Diffusion in the hard sphere fluid. *Mol. Phys.*, **62**, 509 (1987).
[41] J.P. Hansen, L. Verlet. Phase transitions of the Lennard-Jones system. *Phys. Rev.*, **184**, 151 (1969).